Electronic Supplementary Material (ESI) for Nanoscale.

Supporting Informantion

Hierarchical Whisker-on-sheet NiCoP with Adjustable Surface structure for Efficient Hydrogen Evolution Reaction

Zhicheng Cai, Aiping Wu, Haijing Yan, Yinglu Xiao, Congfang Chen, Chungui Tian, Lei Wang, Ruihong Wang and Honggang Fu**

Key Laboratory of Functional Inorganic Material Chemistry, Ministry of Education, Heilongjiang University, Harbin 150080, People's Republic of China
Fax: (+86 451 8667 3647)

E-mail: fuhg@vip.sina.com; fuhg@hlju.edu.cn; chunguitianhq@163.com

Supporting Informantion

Contents

11. Figure S10. The ECSA normalized LSV curves of S15P and S15P-A30

12. Figure S11. LSV curves of S15P-A30 after test of 48 h.

13. Figure S12. a) Polarization curves and b) Tafel plots of S15P, S10T80P, S10T120P and S15P-A30 electrodes for HER with iR-correction.

14. Figure S13. HER polarization curves of S15P-A30 from surface activation of S15P with 2 M, 3 M and 4 M KOH for 30 min.

15. Figure S14. Polarization curves of the catalysts from surface activation of S15P by3M KOH for 10 min (S15P-A10), 30 min (S15P-A30), 60 min (S15P-A60) and 120 min (S15P-A120).

16. Figure S15. The polarization curves of S15P, S10T80P, S10T120P and S15P-A30 for HER (a) in acidic medium (0.5 M H_2SO_4) and (b) neutral medium.

17. Figure S16. Wetting-ability testing of Ni foam.

18. Figure S17. FTIR spectra of S15P and S15P-A30

19. Figure S18. Polarization curves for S15P, S15P-A30, S15P-KCl and S15P-NaOH

20. Figure S19. Nyquist plots of S15P and S15P-A30 electrodes. Inset: the corresponding equivalent circuit diagram consisting of an electrolyte resistance (Rs), a charge-transfer resistance (Rct), and a constant-phase element (CPE).

21. Figure S20. The work function values of Ni foam.

22. Figure S21. Polarization curves of S15P, S15P-A10, S15P-A30, S15P-A60 and S15P-120 for OER.

23. Figure S22. Polarization curves of HWS NiCo-precursor, S15P, S15P-A10, S10T80P and S10T120P electrodes for OER.

24. Figure S23. Polarization curves of S15P-A10 before and after carrying out 3000 CV cycles in 1.0 M KOH. Inset: the curve of current density vs time for S15P-A10 at

a constant potential of 340 m V for 48 h.

25. Figure S24 a) Polarization curves of the electrodes by using S15P-A10||S15P-A30 cell in 1 M KOH with a scan rate of 2 mV/s; b) Chronoamperometric curves for S15P-A10||S15P-A30 cell in 1M KOH at current density of 50 mA/cm^2 over 48 h

Table S2. XPS quantification report of S15P and S15P-A30.

Video S1. Video of water being drawn on the surface of S15P.

Video S2 Video of water being drawn on the surface of S15P-A30.

Video S3 Video of water being drawn on the surface of NiCo-precursor.

Table S1. Comparison of HER activity of HWS NiCoP-A30 with other reported catalysts for HER in alkaline media.

Catalyst	**Electrolyte**	**Massloading (mg/cm^2)**	**Current density (mA/cm^2)**	**Overpotential (mV)**	**Ref.**
Ni_5P_4 films	1.0 M KOH	3.475	10	150	[1]
Ni-P/cp	1.0 M KOH	25.8	10	117	[2]
CoP/rGO	1.0 M KOH	0.28	10	150	[3]
Co-P film	1.0 M KOH	2.6	10	94	[4]
FeP-CFP	1.0 M KOH	2	10	181	[5]
u-CoP/Ti	1.0 M KOH	6.32	10	60	[6]
Ni_2−xCo_xP /rGO	1.0 M KOH	0.15	10	209	[7]
CoP NS/C	1.0 M KOH	0.71	10	111	[8]
CoP-MNA	1.0 M KOH	6.2	10	54	[9]
NiCoP/CC	1.0 M KOH	2	10	62	[10]
$NiCo_2Px$/CF	1.0 M KOH	5.9	10	82	[11]
NiCoP-HQP	1.0 M KOH	5	10	124	[12]

Ni_2P/CP	1.0 M KOH	1	10	85	[13]
CoP	1.0 M KOH	5.57	10	52	[14]
HWS-NiCoP/NF-A30	1.0 M KOH	8	10	42	This work

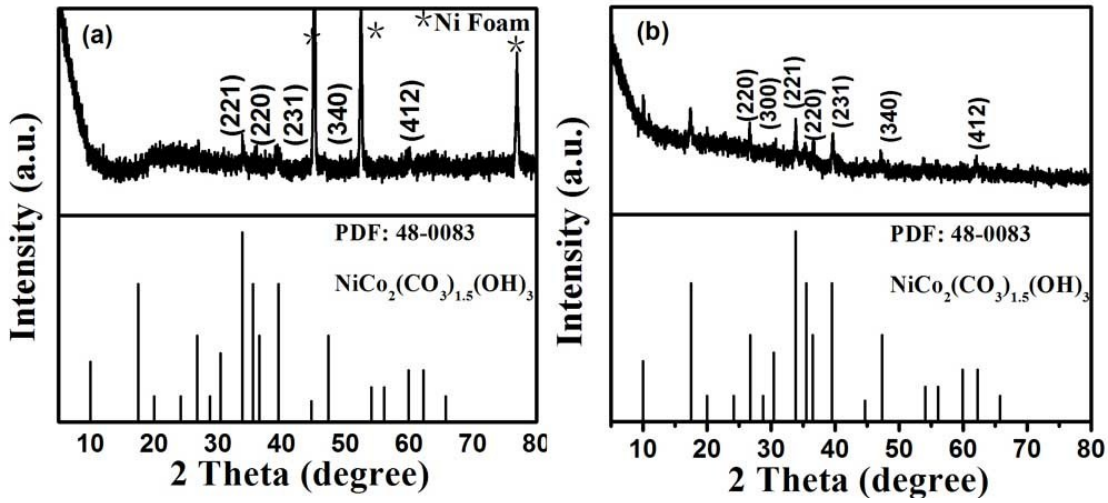

Figure S1. XRD patterns of a) HWS NiCo-precursor/NF and b) HWS NiCo-precursor scraped off from Ni foam.

XRD patterns of NiCo-precursor located on Ni foam is shown in Figure S1a. We can observe the intensive peaks corresponding to metal Ni from Ni foam. The weak peaks in XRD pattern can be indexed to $NiCo_2(CO_3)_{1.5}(OH)_3$ (JCPDS: 48-0083). To exclude the effect of Ni foam, the sample is scraped off from Ni foam and characterized by XRD. As shown in Figure S1b, the peaks are well match with $NiCo_2(CO_3)_{1.5}(OH)_3$ (JCPDS: 48-0083) phase. The results indicate the growth of the $NiCo_2(CO_3)_{1.5}(OH)_3$ on Ni foam after hydrothermal treatment of $Ni(NO_3)_2 \cdot 6H_2O$,

$Co(NO_3)_2 \cdot 6H_2O$ in the presence of NH_4F and $CO(NH_2)_2$.

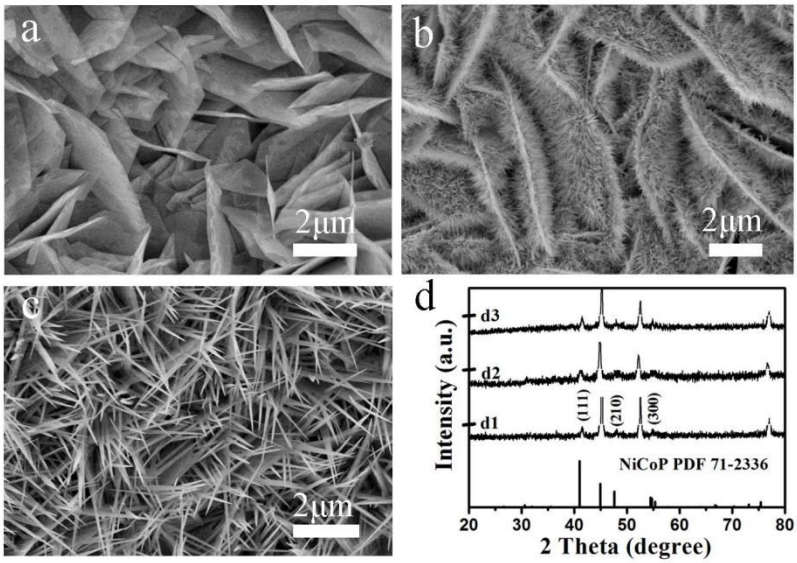

Figure S2. The SEM images of a) S10T80P, b) S15P and c) S10T120P; XRD patterns of d1) S10T80P, d2) S15P and d3) S10T120P.

The typical precursor with sheet-like (S10T80), whisker-on-sheet like (S15), and wire-like (S10T120) morphology were phosphatized to give NiCoP with different structure. We can see that the morphology of the precursor can be remained by controlling the phosphatization condition, and NiCoP with sheet-like (S10T80P), whisker-on-sheet like (S15P) and wire-like (S10T120P) can be obtained. The XRD of T80S10P, S15P and T120S10P are similar, in which the intensive peaks corresponding to Ni are observed in company with weak peaks of NiCoP (Figure S2d).

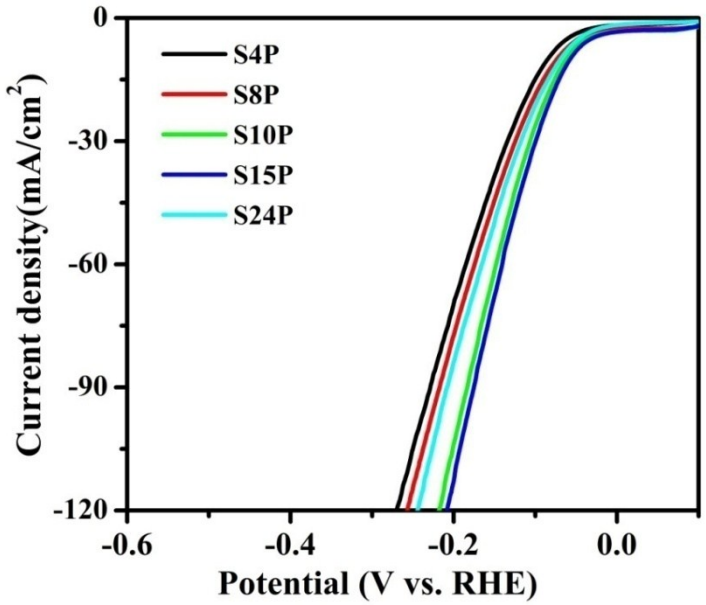

Figure S3. Polarization curves for S4P, S8P, S10P, S15P and S24P tested in 1.0 M KOH at a scan rate of 2.0 mV /s.

The LSV curves of S4P, S8P, S10P and S24P in 1.0 M KOH are shown in Figure S3. Apparently, the S15P has optimal HER performance with η_{10} of 59 mV, followed by S10P (η_{10} of 63 mV), S24P (η_{10} of 70 mV), S8P (η_{10} of 74 mV), S4P (η_{10} of 85 mV) (the phosphorization temperature is 325^{o}C).

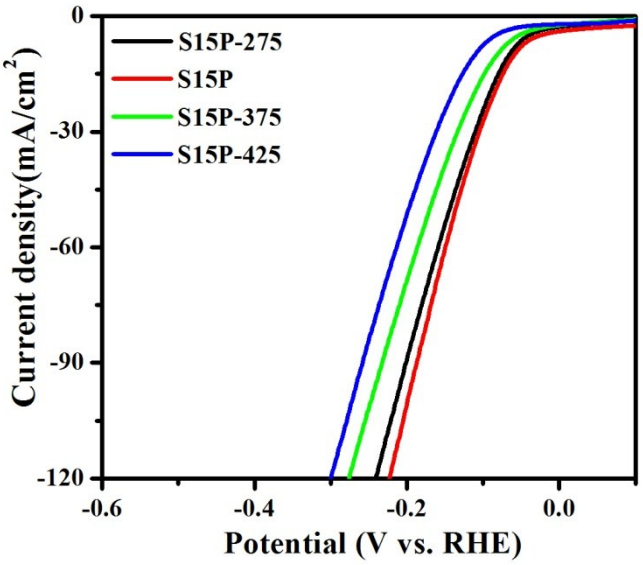

Figure S4. Polarization curves for samples from the phosphorization of HWS NiCo-precursor at 275^{o}C (S15P-275), 325^{o}C (S15P), 375^{o}C (S15P-375) and 425^{o}C (S15P-425) tested in 1.0 M KOH with a scan rate of 2.0 mV/s.

Figure S4 shows HER activity of samples from the phosphorization of HWS NiCo-precursor at 275^{o}C (S15P-275), 325^{o}C (S15P), 375^{o}C (S15P-375) and 425^{o}C (S15P-425) tested in 1.0 M KOH with a scan rate of 2.0 mV/s. The η_{10} are 65, 59, 80 and 109 mV for S15P-275, S15P, S15P-375 and S15P-425, respectively. The results indicate that 325^{o}C is the optimal phosphorization temperature for the synthesis of NiCoP with optimized HER activity.

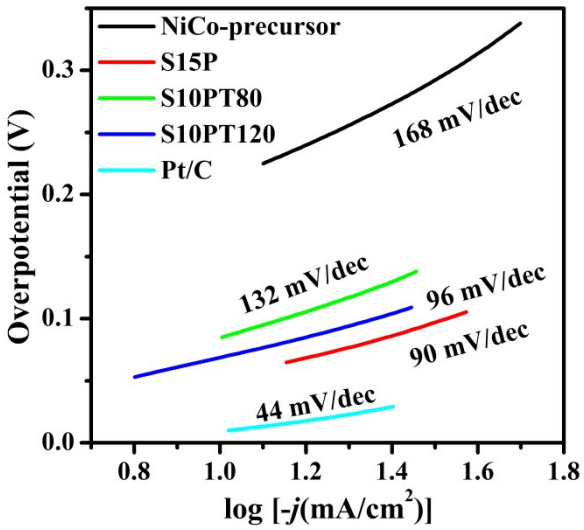

Figure S5. Tafel plots of HWS NiCo-precursor, S15P, Pt/C, S10T80P and S10T120P.

Tafel plots for HWS NiCo-precursor, S15P, Pt/C, S10T80P and S10T120P samples are 168 mV/dec, 90 mV/dec, 44 mV/dec, 132 mV/dec and 96 mV/dec. The Pt/C has given the low Tafel values. Also, we can see all of NiCoP samples show the better activity than HWS NiCo precursor, implying the importance of the phosphidation for improving the performance of the catalyst. Among all of NiCoP samples, the S15P shows the lowest Tafel values, implying it has most favorable HER dynamics.

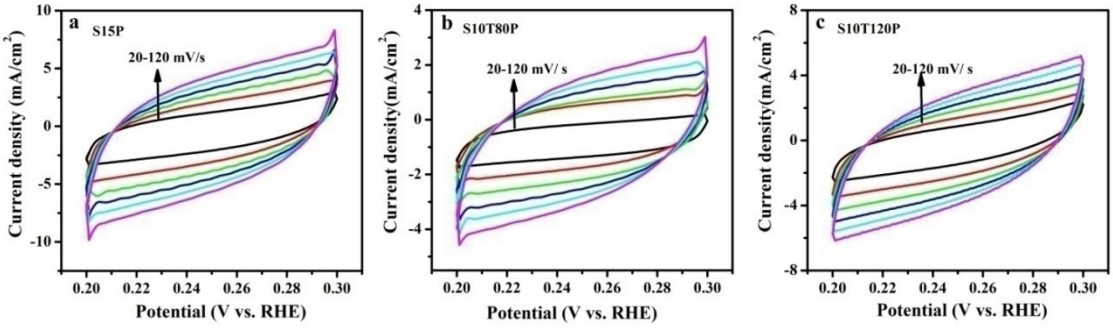

Figure S6. ECSA of S15P, S10T80P and S10T120P electrode measured by cyclic voltammograms at different scan rates from 20 to 120 mV/s.

Figure S6 shows cycle voltammetry (CV) curves carried out from 200 to 300 mV with scan rates from 20 to 120 mV/s. The S15P exhibits a C_{dl} of 31.34 mF/cm^2 in alkaline media, much higher than those of NiCoP nanosheet (S10T180P, 16.39 mF/cm^2) and nanowires (S10T120P, 22.08 mF/cm^2). The results show that S15P has more active sites, which is favorable to enhance HER performance.

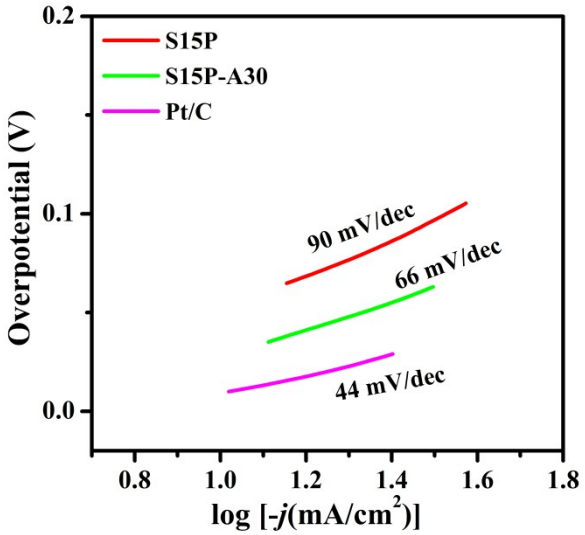

Figure S7. Tafel plots of S15P, S15P-A30 and Pt/C.

Figure S7 shows Tafel plots of S15P, S15P-A30 and Pt/C. We can see that S15P-30A shows lower tafel slopes of 66 mV/dec than that of S15P (90 mV/dec), implying the improved HER dynamics on S15P-30A samples. It also demonstrates the importance of surface activition on improving the performance of the catalyst.

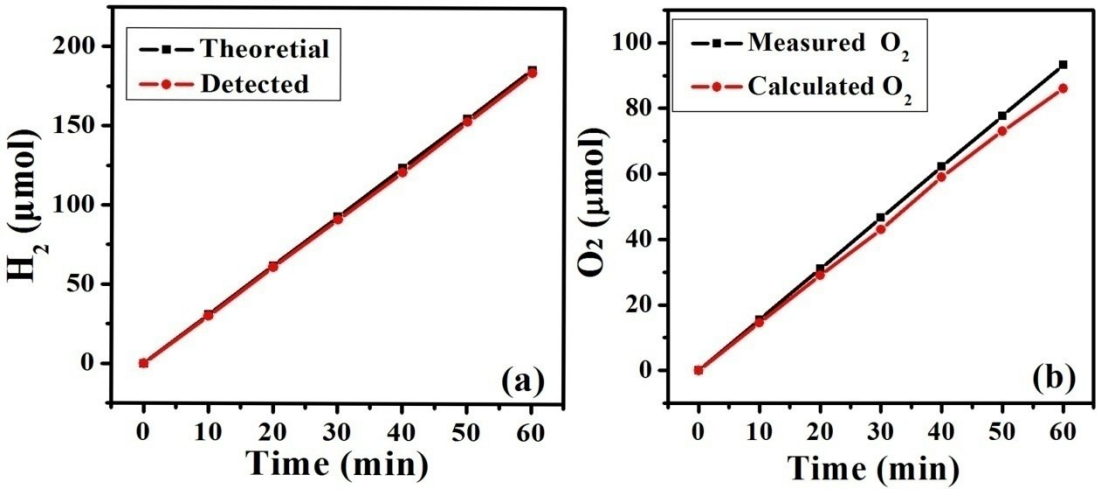

Figure S8. The Faradiac efficiency of (a) HER of S15P-A30 and (b) OER of S15P-A10

The Faradiac efficiency of catalyst for HER of S15P-A30 and OER of S15P-A10

is about 100% and 93% at 60 min of test.

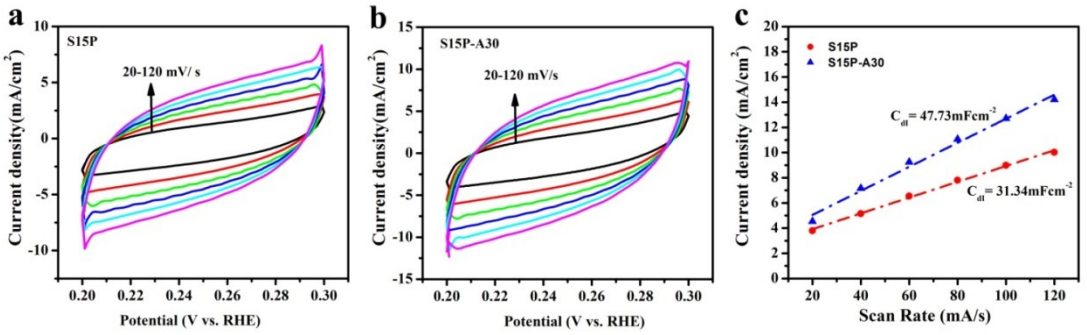

Figure S9. The ECSA of a) S15P and b) S15P-A30 measured by cyclic voltammograms at different scan rates from 20 to 120 mV/s; c) is corresponding curve of current densities of S15P and S15P-A30 as a function of scan rate.

Based on the test of cyclic voltammograms (Figure S9a, b), we can see that that the S15P-A30 exhibited higher ECSA (C_{dl}= 47.73 mF/cm^2) than S15P (C_{dl} =31.34 mF/cm^2) in alkaline media.

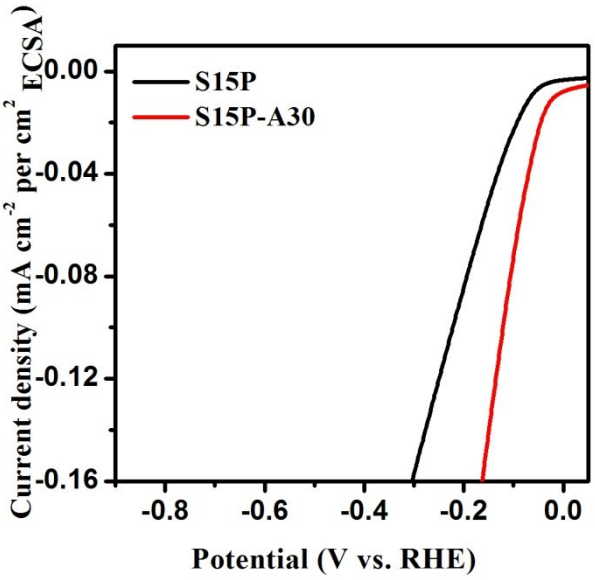

Figure S10. The ECSA normalized LSV curves of S15P and S15P-A30

The ECSA normalized LSV curves of S15P and S15P-A30 are shown in Figure S10. It is obvious that the S15P-A30 shows a superior normalized activity than S15P sample.

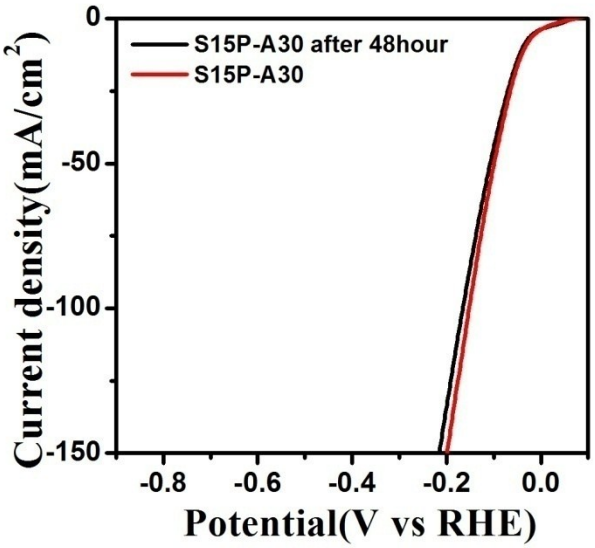

Figure S11. LSV curves of S15P-A30 after test of 48 h.

Figure S11 shows LSV curves of S15P-A30 after test of 48 h. It is shown that the samples shown the good stability for long-time test (Figure S11). The activity of the catalyst decay should be relative with the slight detachment of the catalyst from NF caused by generation of gas, and the excessive reaction of electrolyte (KOH) with NiCoP.

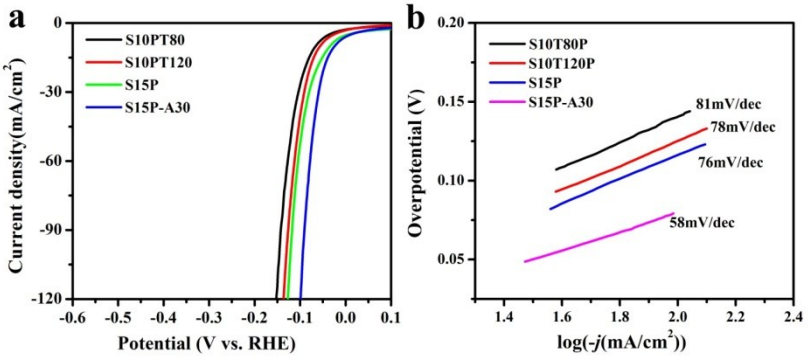

Figure S12. a) Polarization curves and b) Tafel plots of S15P, S10T80, S10T120 and S15P-A30 for HER with iR-correction.

Figure S12 shows the polarization curves and Tafel plots of S15P, S10T80P, S10T120P and S15P-A30for HER with iR-correction. The overpotentials to reach 10

mA/cm^2 are 42, 76, 63 and 31 mV forS15P, S10T80, S10T120 and S15P-A30 catalyst. The corresponding Tafel plots were 76, 81, 78 and 58 mV/dec, respectively. With iR-correction, we can see that the S15P-A30 given lowest η_{10} close to Pt/C and lowest Tafel values, further demonstrating the role of surface activition by KOH on the improvement of the performance.

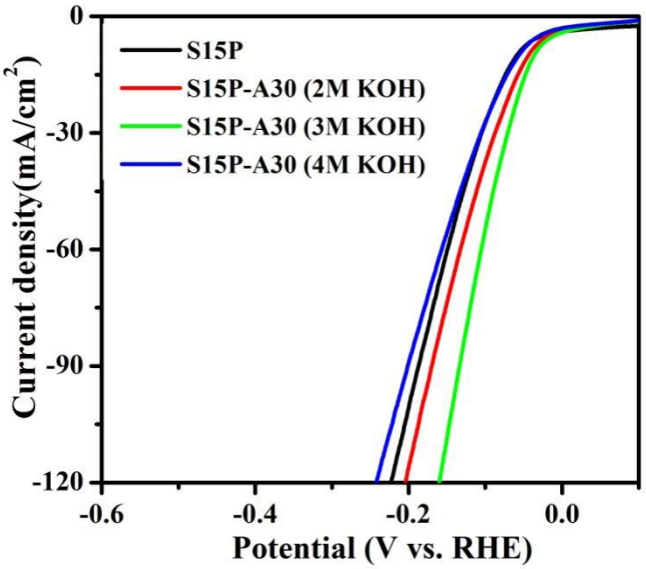

Figure S13. Polarization curves of S15P-A30 from surface activition of S15P by 2M KOH (S15P-A30 (2M KOH)), 3 M KOH (S15P-A30 (3 M KOH)) and 4 M KOH (S15P-A30 (4 M KOH)) KOH for 30 min.

Figure S13 shows polarization curves of S15P-A30 from surface activation of S15P by 2 M, 3 M and 4 M KOH for 30 min. The overpotentials are 46, 42 and 56 mV to drive the current densities of 10 mA/cm^2 for S15P-A30 (2 M KOH), S15P-A30 (3 M KOH), S15P-A30 (4 M KOH).The S15P-A30 (3 M KOH) from surface activation of S15P by 3M KOH, shows the best HER performance. The use of low concentrated KOH will result in the incomplete activation of S15P, while the high concentrated KOH can results the damage of the catalyst. So, the selection of KOH with suitable concentration is very important for realizing effective activation.

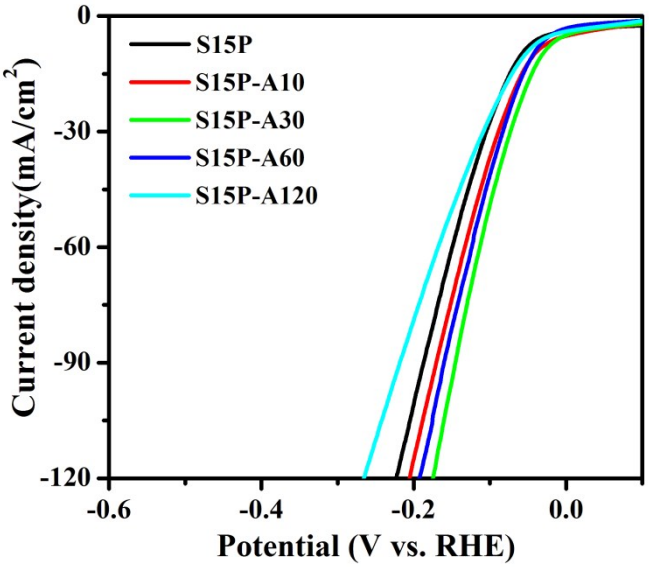

Figure S14. Polarization curves of the catalysts from surface activation of S15P by 3 M KOH for 10 min (S15P-A10), 30 min (S15P-A30), 60 min (S15P-A60) and 120 min (S15P-A120).

Figure S14 shows polarization curves of the catalysts from surface activition of S15P by 3M KOH for 10 min (S15P-A10), 30 min (S15P-A30), 60 min (S15P-A60) and 120 min (S15P-A120). We can see that the overpotentials to reach current density of 10 mA/cm^2 are 44, 42, 48 and 54 mV for S15P-A10, S15P-A30, S15P-A60 and S15P-A120. The S15P-A30 showed the best HER activity. The short activition time will result in the incomplete activation of S15P, while the long time can results the damage of the catalyst. So, the selection of KOH with suitable activition time is very important for realizing effective activation.

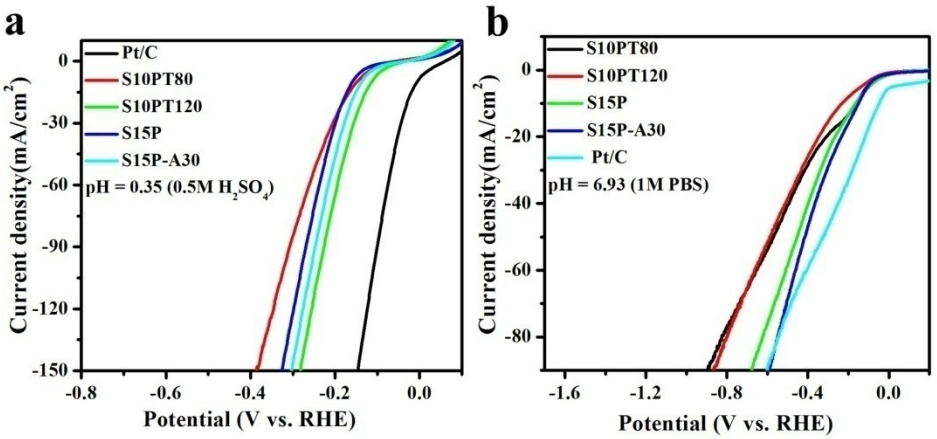

Figure S15. The polarization curves of S15P, S10T80P, S10T120P and S15P-A30 for HER (a) in acidic medium (0.5 M H_2SO_4) and (b) neutral medium.

Figure S15 shows the polarization curves of S15P, S10T80, S10T120 and S15P-A30 electrodes for HER in acidic medium (0.5 M H_2SO_4) and neutral medium (1 M PBS PH=6.93). The overpotentials to achieve the current density of 10 mA/cm^2 are 135 and 149 mV for S15P-A30 in 0.5 M H_2SO_4 and 1 M PBS, respectively. The result indicates the S15P-A30 owns superior actvity for HER in broad pH range.

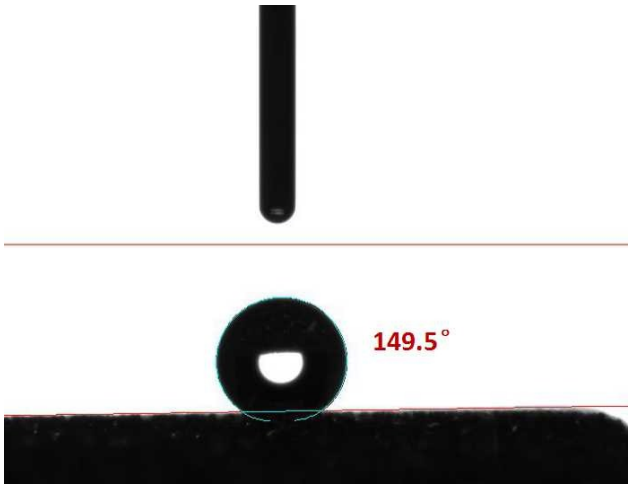

Figure S16. Wetting-ability testing of Ni foam. The contact angle of 149.5°for Ni foam indicates the hydrophobic characteristic. The wetting-ability of HWS NiCoP

and S15P-A30 was shown in Video S1, S2 and S3.

The surface of the Ni foam is hydrophobic property with 149.5° of water contact angles. In contrast, water drop on HWS NiCo-precursor and HWS NiCoP spread out in 0.6 s (Video S3) and 0.24 s, respectively. The results indicate the enhancement of surface wettability after growth of HWS NiCo-precursor, especially of HWS NiCoP. The improvement of wetting-ability should be ascribed to the special hierarchical whisker-on-sheet structure favorable to spread the water drop. Notably, the water drop spread out only in 0.2 s on S15P-A30, faster than on S15P. It is obvious that hydrophilic properties is largely improvement after surface activation treatment, which should be favourable to the improvement of catalytic activity.

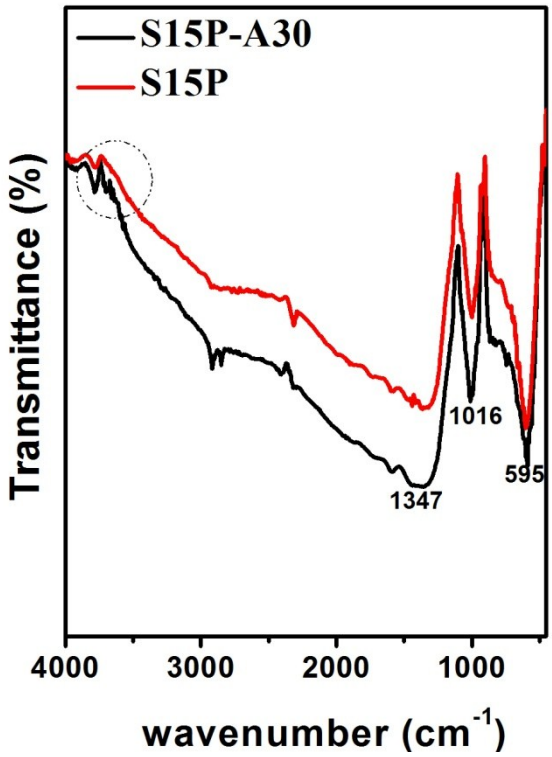

Figure S17. FTIR spectra of S15P and S15P-A30

Figure S17 shows the FT-IR spectra of the sample scraped off from the Ni foam. There are no emergency of new peaks for sample after surface activation. However, by comparison, we have found the peak located at about 3700 cm^{-1}, ascribing to

stretching vibration of hydroxyl groups (ν O–H), have slight increase for S15P-30A sample. This should be relative with a increase of surface –OH after activation.

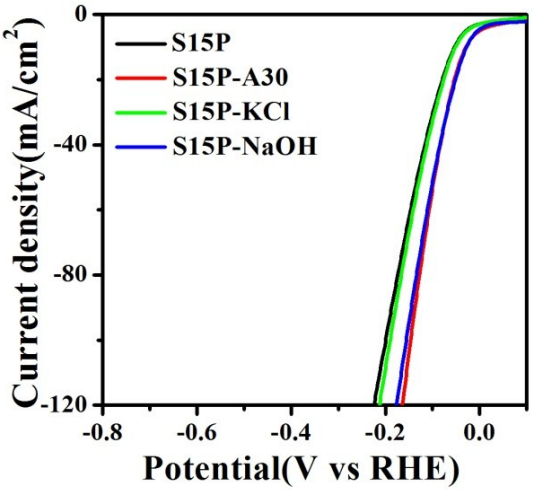

Figure S18. Polarization curves for S15P, S15P-A30, S15P-KCl and S15P-NaOH tested in 1.0 M KOH at a scan rate of 2.0 mV /s.

In contrast, S15P-KCl was treatment by 3M KCl and S15P-NaOH was treatment by 3M NaOH. KCl has no obvious effect on the catalytic activity. The experiments indicate the important role of –OH in solution for surface activation.

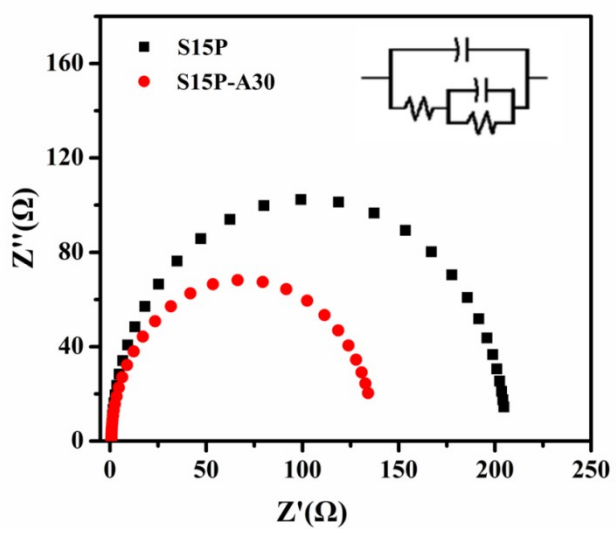

Figure S19. Nyquist plots of S15P and S15P-A30. Inset is corresponding equivalent

circuit diagram consisting of an electrolyte resistance (Rs), a charge-transfer resistance (Rct).

The electrochemical impedance spectroscopy (EIS) analysis is applied for studying the effect of surface activation on the kinetics of HER. It can be seen that the S15P-A30 samples exhibited the lower Rct comparing with that of S15P, indicating S15P-A30 has low internal resistance.

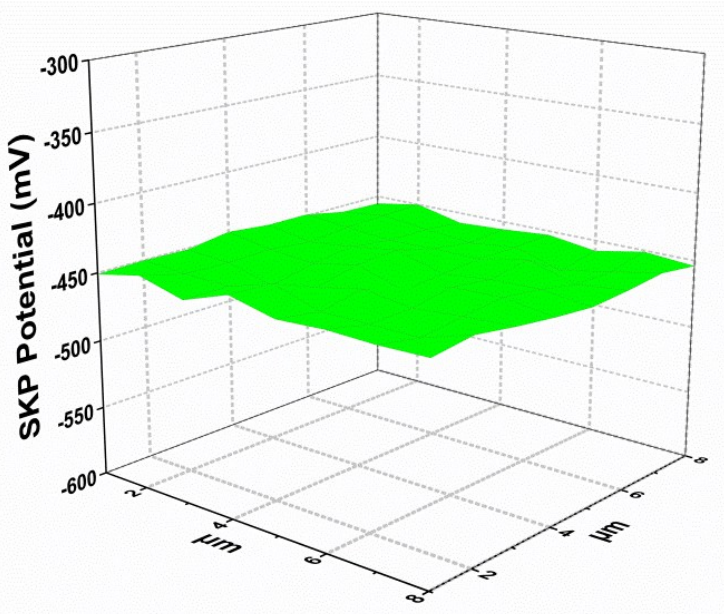

Figure S20. The work function values of Ni foam

The work function values of Ni foam is about 4.89 eV.

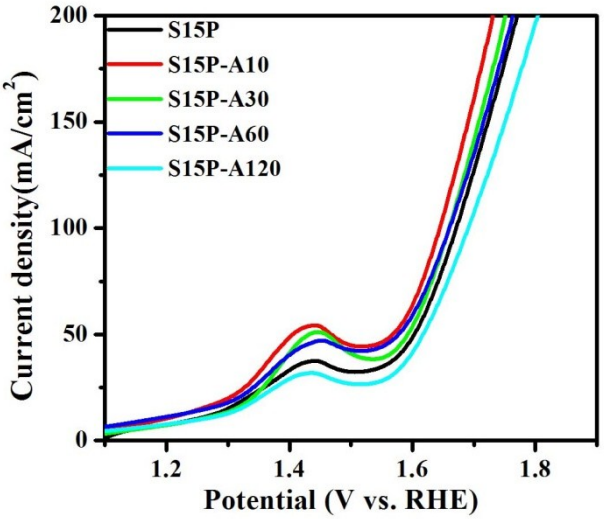

Figure S21. Polarization curves of S15P, S15P-A10, S15P-A30, S15P-A60 and S15P-120 for OER in 1 M KOH.

Figure S21 shows the polarization curves of S15P, S15P-A10, S15P-A30, S15P-A60 and S15P-A120 electrodes for OER in alkali medium (1 M KOH). The corresponding overpotentials to achieve the current density of 100 mA/cm^2 are 440, 410, 428, 431 and 460 mV, respectively. The result indicates the S15P-A10 can be used as superior catalyst for OER.

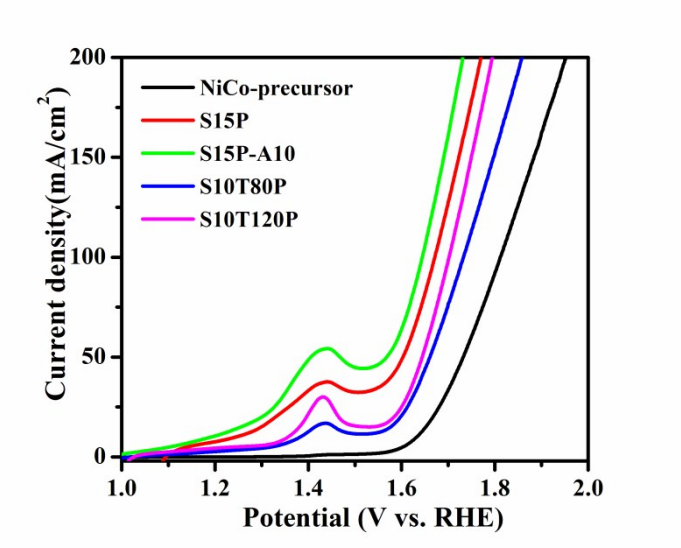

Figure S22. Polarization curves of NiCo-precursor, S15P, S15P-A10, S10T80P, and S10T120P electrodes for OER in KOH.

Figure S22 shows the polarization curves of NiCo-precursor, S15P, S15P-A10

S10T80P and S10T120P electrodes for OER in alkaline medium. The corresponding overpotentials to achieve the current density of 100 mA/cm^2 are 597, 440, 410, 504, and 469 mV, respectively. The result indicates the S15P-A10 can be used as superior catalyst.

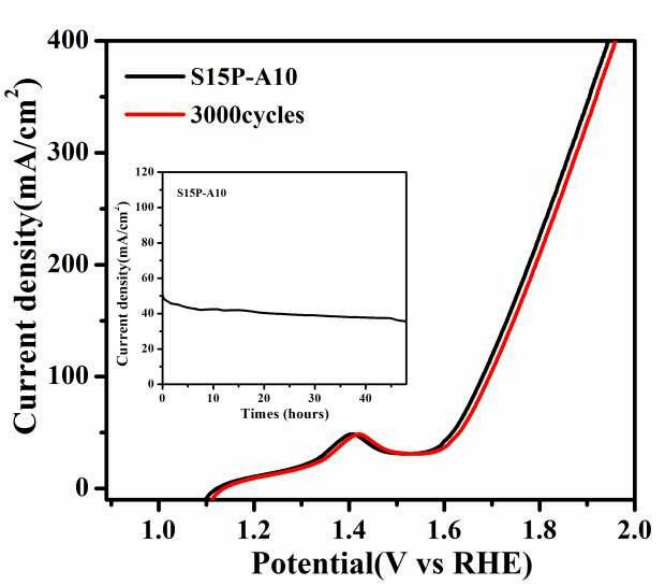

Figure S23. Polarization curves of S15P-A10 before and after carrying out 3000 CV cycles in 1.0 M KOH. Inset: the curve of current density *vs* time for S15P-A10 at a constant potential of 340 m V for 48 h.

The OER stability of S15P-A10 was tested. Figure S23 show the OER of S15P-A10 before and after carrying out 3000 cycles of the CV measurement in 1.0 M KOH. As shown in inset, S15P-A10 electrode under a static overpotential of 340 mV after 48 h. There is no obvious loss of current density after 48 h, also indicates that S15P-A10 is stable in a long term electrochemical OER process.

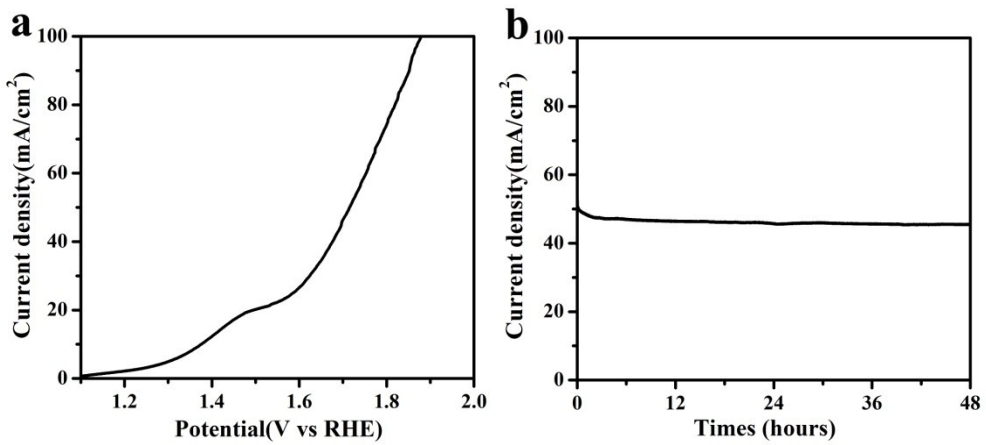

Figure S24. a) Polarization curves of S15P-A10||S15P-A30 cell in 1 M KOH with a scan rate of 2 mV/s; b) Chronoamperometric curve for S15P-A10||S15P-A30 cell in 1 M KOH at current density of 50 mA/cm^2 over 48 h.

Based on the high activity of the catalyst for HER and OER, we built an overall water splitting device by using S15P-A30 as cathode and S15P-A10 as anode in alkali medium. The activity of water electrolysis was evaluated by the current-potential response in 1 M KOH. The S15P-A only needs a cell voltage of ~1.72 V at current density of 50 mA/cm^2 (Fig. S24a), in the meantime, S15P-A shows good stability go through long-term testing after 48 h as shown in Figure S24b.

Table S2. XPS quantification report of S15P and S15P-A30.

Sample	Peak	Position BE (eV)	FWHM	Raw Area (cps eV)	Atomic Mass	Atomic Conc %
S15P	Ni $_{2p}$	855.650	2.952	17069.9	58.702	16.95
S15P	Co $_{2p}$	780.450	3.482	6683.7	58.933	7.78
S15P	O $_{1s}$	530.700	1.983	8145.4	15.999	49.43
S15P	C $_{1s}$	284.600	1.735	1113.9	12.011	21.56
S15P	P $_{2p}$	133.750	1.625	667.2	30.974	9.80
S15P-A30	Ni $_{2p}$	856.850	2.102	3965.5	58.702	4.93
S15P-A30	Co $_{2p}$	781.550	3.351	3172.5	58.933	4.62
S15P-A30	O $_{1s}$	532.550	2.916	7561.3	15.999	57.40
S15P-A30	C $_{1s}$	284.600	1.482	959.4	12.011	23.26
S15P-A30	P $_{2p}$	128.850	0.973	364.7	30.974	4.28

Supplementary videos

Video S1 Video of water drops being drawn into the surface of S15P

Video S2 Video of water drops being drawn into the surface of S15P-A30.

Video S3 Video of water being drawn on the surface of NiCo-precursor.

Reference

[1]. M. Ledendecker, S. Krick Calderon, C. Papp, H. P. Steinruck and Shalom, M. *Angew. Chem*., 2015, **54**, 12361-12365.

[2]. X. Wang, W. Li, D. Xiong, D. Y. Petrovykh and L. Liu, *Adv. Funct. Mater.*, 2016, **26**, 4067-4077.

[3]. L. Jiao, Y. X. Zhou and H. L. Jiang, *Chem. Sci*., 2016, **7**, 1690-1695.

[4]. N. Jiang, B. You, M. Sheng and Y. Sun, *Angew. Chem.*, 2015, **54**, 625-6254.

[5]. C. Lv, Z. Peng, Y. Zhao, Z. Huang and C. Zhang, *J. Mater. Chem. A*, 2016, **4**, 1454-1460.

[6]. D. Zhou, L. He, W. Zhu, X. Hou, K. Wang, G. Du, C. Zheng and X. Sun, A. M. Asiri, *J. Mater. Chem. A*, 2016, **4**, 10114-10117.

[7]. J. Li, M. Yan, X. Zhou, Z. Q. Huang, Z. Xia, C. R. Chang, Y. Ma and Y. Qu, *Adv. Funct. Mater*., 2016**, 26**, 6785-6796.

[8]. X. Wang, Y. V. Kolen'ko, X. Q. Bao, K. Kovnir and L. Liu, *Angew. Chem.*, 2015, **54**, 8188-8192.

[9]. Y. P. Zhu, Y. P. Liu, T. Z. Ren and Z. Yuan, *Adv. Funct. Mater*., 2015, **25**, 7337-7347.

[10]. C. Du, L. Yang, F. Yang, G. Cheng and W. Luo, *ACS Catalysi*s, 2017, **7**, 4131-4137.

[11]. R. Zhang, X. Wang, S. Yu, T. Wen, X. Zhu, F. Yang, X. Sun, X. Wang and W. Hu, *Adv. Mater*., 2017, **29**, 1605502.

[12]. Y. Li, J. Liu, C. Chen, X. Zhang and J. Chen, *ACS Appl. Mater. Inter.*, 2017, **9**, 5982-5991.

[13]. P. W. Menezes, A. Indra, C. Das, C. Walter, C. Göbel, V. Gutkin, D. Schmeiβer and M. Driess, *ACS Catal*., 2016, **7**, 103-109.

[14]. J. Huang, Y. Li, Y. Xia, J. Zhu, Q. Yi, H. Wang, J. Xiong, Y. Sun and G. Zou, *Nano Res*., 2017, **10**, 1010-1020.